Available online at www.sciencedirect.com
SCIENCE DIRECT
Trans. Nonferrous Met. Soc. China 16(2006) 1015−1020
Transactions of Nonferrous Metals Society of China
www.csu.edu.cn/ysxb/

FEA modeling of effect of axial feeding velocity on strain field of rotary swaging process of pure magnesium

RONG Li(荣 莉), NIE Zuo-ren(聂祚仁), ZUO Tie-yong(左铁镛)

School of Material Science and Engineering, Beijing University of Technology, Beijing 100022, China

Received 16 November 2005; accepted 15 June 2006

Abstract: A coupled thermal-mechanical model of the rotary swaging of pure magnesium was developed using the general finite-element software program MSC/Marc to visualize the effect of axial feeding velocity on the rotary swaging process. The radial displacement occurring in one pulse impact increases in proportion to axial feeding velocity (v_{ax}). When the other processing parameters are fixed, the surface roughness of the swaged bar increases with v_{ax} and is in parabolic relation with v_{ax}. There exists a minimum velocity $v_{ax,\,min}$ below which the decrease of v_{ax} will no longer improve the surface roughness. Under the technological conditions of this simulation, when the finial diameter d=6.6 mm, $v_{ax,\,min}$=1.82 m/min, and when d=7.0 mm, $v_{ax,\,min}$=1.83 m/min. If R_a=3.2 is required for the end product, then $v_{ax,\,max}$=6.02 m/min is gotten for d=6.6 mm and $v_{ax,\,max}$=7.05 m/min for d=7.0mm. The increase of v_{ax} has no notable influence on strain distribution along radial direction. The errors between the experimental and simulated height of the spiral spine-like ridges are below 8.0%.

Key words: rotary swaging; magnesium; strain filed; processing parameters

1 Introduction

Rotary swaging, which has properties of pulse forging and multidimensional beating, has high deformation efficiency and provides compressive stress state which benefits brittle material deformation[1]. On the other hand, magnesium wires are up to date fabricated mainly by casting and extrusion[2]. However, the as-cast magnesium wires have poor mechanical properties and inferior surface finish quality, and the as-extruded magnesium wires are not widely used because of its low deformation efficiency and insufficient strength. So it is important to develop a new process to fabricate magnesium wires. Researches on swaging of magnesium offers good opportunity to improve the magnesium wire fabrication.

In recent years, the study on conventional spin forming[3], sheet metal forming[4−6], extrusion[7] and superplasticity[8] of magnesium and its alloys has been reported. However, rotary swaging of pure magnesium has not been reported. There are some FEA of the swaging process, but reports on FEA of the rotary swaging process with the characteristic of pulse loading are rare.

Axial feeding velocity which is the distance the chuck jaw moves in unit time, directly influences the surface quality and production efficiency. In the article the effect of axial feeding velocity on pure magnesium swaging was studied through experiment and FEA simulation to provide theoretical information for implementing of pure magnesium rotary swaging.

2 Numerical modeling of rotary swaging processing

2.1 Finite element model definition

A schematic view of the swaging machine head are shown in Refs.[1]. The geometric parameters of swaging die segments are shown in Fig.1(a). The workpiece moves in both radial and axial directions. So in the FEM of swaging the die segment is defined as rigid contact body and the swaging processing parameters, such as radial displacement and axial feeding velocity, are adjusted by changing moving curves of the rigid body.

Considering the axial symmetry of both the loads and the workpiece, 1/2 of the axial section is analyzed in

Foundation item: Project(98009999200301) supported by the Ministry of Science and Technology of China
Corresponding author: NIE Zuo-ren; Tel: +86-10-67391536; E-mail: zrnie@bjut.edu.cn

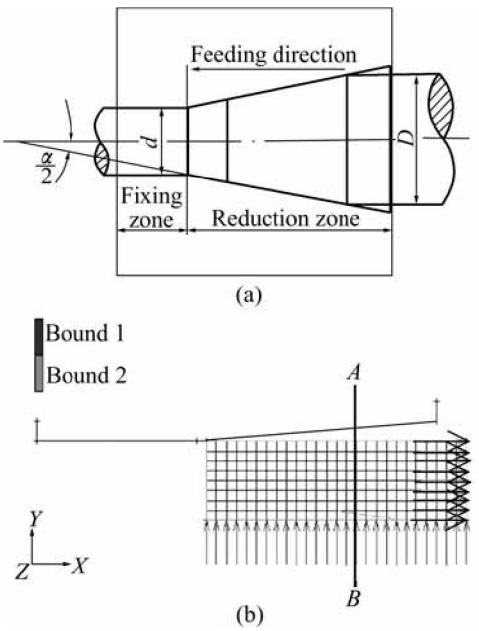

Fig.1 Geometric parameters of swing die segments(a) and geometric modeling and initial meshes of swaging(b)

the FEA model. No.10 four-node, axisymmetric, quadrilateral full integration elements are chosen to develop FEA model of rotary swaging. Initial meshes and mechanical boundary conditions are shown in Fig.1(b). All related mechanical and thermal properties are functions of temperature and input according to ASTM handbook[9]. Flow stress curves obtained through experiments[10] are edited as a material data file which would be read by MSC.Marc in simulation[11].

2.2 Initial conditions and boundary conditions

The mechanical boundary conditions are as follows: based on the deformation nature of swaging, the radial displacement of nodes at the axis of the workpiece and the axial displacement of nodes at the right end face of the workpiece are set as zero. The conditions at the interfaces between the workpiece and dies were described using the Coulomb friction model and the friction coefficient is 0.25.

The thermal boundary conditions are as follows: as the measured temperature-fluctuation during experiments of pure magnesium swaging is small, the radiation heat-transfer coefficient changes insignificantly. So the rate of heat flow due to surface emission and convection is uniformly set as[12]

$$q''=q''+q''_{\mathrm{rad}}=h_1(T-T_\infty)+h_r(T-T_{\mathrm{sur}})=h(T-T_\infty) \quad (1)$$

where h_1 is the convection heat-transfer coefficient, h_r is the radiation heat-transfer coefficient, h is the equivalent heat-transfer coefficient, T is the temperature of swaging workpiece, and T_∞ is the ambient temperature. In the simulation the contact heat transfer coefficient is set as 3 kW/(m^2·K) and the equivalent heat-transfer coefficient is set as 20 W/(m^2·K)[13]. 90% of inelastic deformation associated with mechanical work is converted into heat which will affect temperature distribution. The heat generated from friction is averagely distributed to the workpiece and the dies. The ambient temperature is 25 ℃ and the die segments are preheated to 120 ℃.

2.3 Local adaptive meshing

During rotary swaging processing the loads pulse periodically and so the obvious characteristic of rotary swaging is periodic large local stress, the adaptive criteria based upon absolute testing using equivalent von mises stress is used. In this way, an element is subdivided if Eqn.(2) is not satisfied:

$$\sigma_{\mathrm{vm}}>f \quad (2)$$

where σ_{vm} is the equivalent stress of any element, f is the coefficient set by authors according to the computing context.

2.4 FEA conditions and determination of loadcase

Table 1 lists the used process parameters which are the same as those of actual swaging machine. The total loading time varies with the magnitude of the axial feeding velocity on the principle of ensuring that the workpiece pass through the whole die longitudinal section. Fixed stepping procedures are adopted and the steps in one pulse impact varies with the magnitude of axial feeding velocity on the principle of ensuring the pulse apex of the moving curve of the rigid body be exactly an end-point of one step.

Table 1 Process parameters used in simulation

Parameter	Value				
Starting diameter, D/mm	8.0				
Ending diameter, d/mm	7.0			6.6	
Axial feeding velocity, v_{ax}/(m·min^{-1})	2.2	3.3	4.0	4.5	5.5
Time cost in one impact, t/s	0.009				
Length of cross-section reduction zone, L_c/mm	12.0				
Length of cross-section fixing zone, L_f/mm	8.0				
Conical feeding angle, α/(°)	19°				
Initial forging temperature/℃	250 ℃				

Model number of swaging machine is B202.

3 FEA results and discussion

3.1 Equivalent strain distribution

The equivalent strain distribution maps after

swaging for 0.12 s are shown in Fig.2. It is found that the deformation zone of swaged bar should be divided into three parts: part Ⅰ is the bulging head-end, Ⅱ is the formed zone and Ⅲ is the reduction zone. In part Ⅱ, the equivalent strain distribution on different sections perpendicular to the axis of the workpiece are the same (the only differences appear on the exterior surface of workpieces which will be clarified in section two of the article) and so the stress & strain distributions of part Ⅱ represents those of finished swaging products. By comparing Fig.2(a) with Fig.2(b), it can be declared that the FE model developed in the article accurately reflects the effect of axial feeding velocity on efficiency, viz. the part of the workpiece that has entered the cross-section fixing zone increases with the enhancement of v_{ax}. When the swaging proceeds for 0.12 s, three parts of deformation zone have appeared at the velocity of 4.5 m/min but at the same time part Ⅱ has not appeared at the velocity of 2.2 m/min.

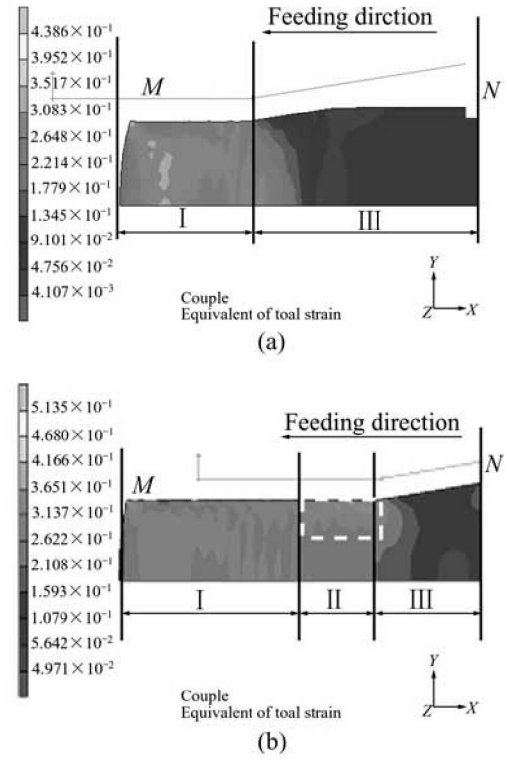

Fig.2 Equivalent strain distribution at swaging time 0.12 s (d=7.0 mm): (a) v_{ax}=2.2 m/min; (b) v_{ax}=4.5 m/min

3.2 Rotary swaging history

In Fig.3, the radial displacements of nodes (see Fig.3(a) for the position of nodes) on section *AB* calculated in the model are plotted as a function of swaging time and pulse impact number at various velocities. The main point to note is that corresponding to the pulse impacting characteristic of swaging, the absolute value of radial displacement of each node increases stepwise and the lasting time of each step is the pulse period of the load. From Fig.3 it is also found that after entering the cross-section fixing zone, the value of radial displacement of each node increases no longer and the value is the final displacement of the node. Comparing plots in Fig.3, it is found that with the increase of v_{ax}, the time taken by the nodes at the same position of the workpieces to finish swaging (see t_1 in Fig.3) decreases and the production efficiency improves. The radial displacement that occurs in one pulse impact h (see h in Fig.3) increases with the enhancement of v_{ax}, and this indicates that when v_{ax} is low, the total deformation of each node is achieved through many times of saddening which benefits the deformation of metals with poor plasticity.

In order to study the relation between axial feeding velocity and 'h', the 'h' of each node on section *AB* is plotted as a function of v_{ax} (see Fig.4), and the correlation coefficient of linear fitting is above 0.997 which indicates that 'h' is in direct proportion to axial feeding velocity.

3.3 Strain distribution along axial direction and effect of v_{ax} on spiral spine-like ridge

Fig.5(a) shows the enlarged view of the broken rectangle zone of Fig.2(b). It is clear that the strain distributes unevenly and local high-strain zones (see the lightest colored triangle marked in Fig.5(a)) arrange periodically along axial direction. This indicates that the strain at exterior surface of the swaging workpiece periodically fluctuates along axial direction. In practical swaging processing, the spiral spine-like ridges at the exterior surface of swaging products are a familiar defect [1,2]. This defect arises from the uneven strain distribution along axial direction and results in periodical fluctuation of the radial displacement along axial direction at exterior surface of swaging products. So the displacement of nodes at exterior surface is plotted as a function of axial coordinates to exactly measure the effect of v_{ax} on the spiral spine-like ridges (see Fig.5(b)).

The marked part Ⅰ in Fig.5(b) corresponds to the exterior surface of the head end of the swaging product, part Ⅱ corresponds to the exterior surface of the formed zone which represents the state of the finish swaging product. At other velocities simulated, the curves of radial displacement changing along axial direction are of the same shape, but the height of the spiral spine-like ridge increases with enhancement of v_{ax}. Increase of the height of the spiral spine-like ridge will result in enlargment of the difference in diameters of sections perpendicular to the axis and so in increasing of surface roughness. So the enhancement of v_{ax} will degrade the surface quality of swaging products.

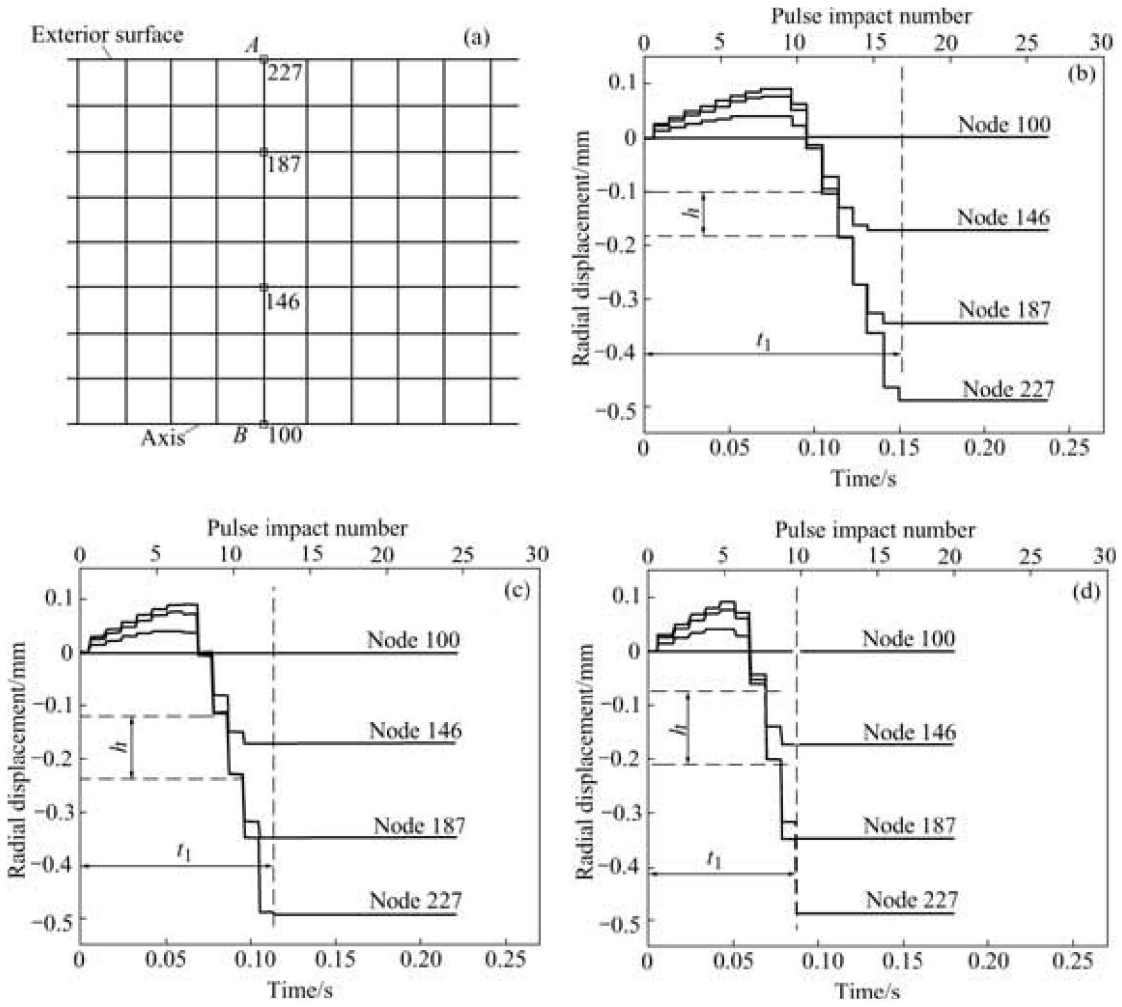

Fig.3 Node position on section *AB* (a) and history plot of radial displacements on various axial feeding velocities (d=7.0 mm): (a) v_{ax}=3.3 m/min; (b) v_{ax}=4.5 m/min; (c) v_{ax}=5.5 m/min

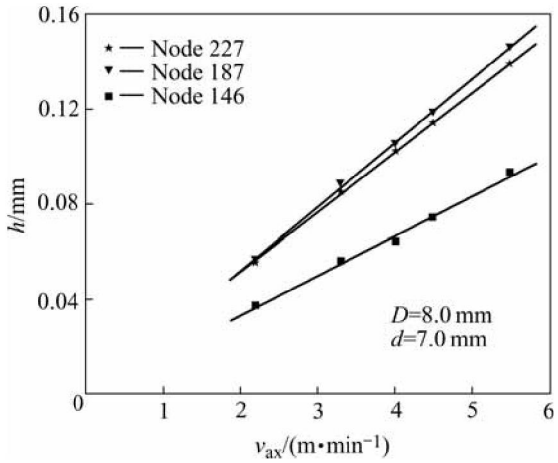

Fig.4 Correlation between h and axial feeding velocity (d=7.0 mm)

3.4 Strain distribution along radial direction

As for nodes at the exterior surface, strain distribution on sections perpendicular to the axis of swaging workpiece are of the same in part Ⅱ, section *AB* (see Fig.1(b) for the position of *AB*) in part Ⅱ is chosen to study the path plot of the equivalent strain along radial direction. Fig.6(a) shows the path plots when ending diameter is 7.0 mm and the digits beside the plots denote the node numbers. It is clear that at various v_{ax}, the plots overlaps but for node 227 and this indicates that v_{ax} has no notable influence on the evenness of the equivalent strain distribution along radial direction. So the magnitude of the axial feeding velocity does not influence the level of the following two defects, viz. pits at the end of the product, and insufficient forging at the core of the swaging products[1]. In addition, the great difference between the equivalent strains of node 227 at various v_{ax} is caused by the defect of the spiral spine-like ridges which lead to local high strain zone at node 227 at the axial velocity of 4.5 m/min and local low strain zone at the axial velocity of 4.0 m/min. Fig.6(b) shows the path plot of the $\bar{\varepsilon}$ along the radial direction when ending diameter is 6.6 mm and from which the same

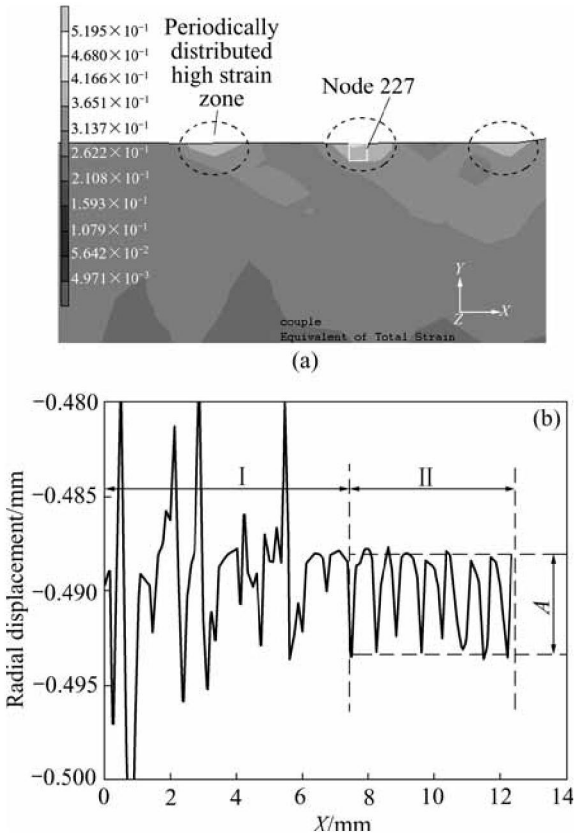

Fig.5 Local equivalent strain distribution (a) and path plot of radial displacement along axial direction (b) (v_{ax}=4.5 m/min, d= 7.0 mm)

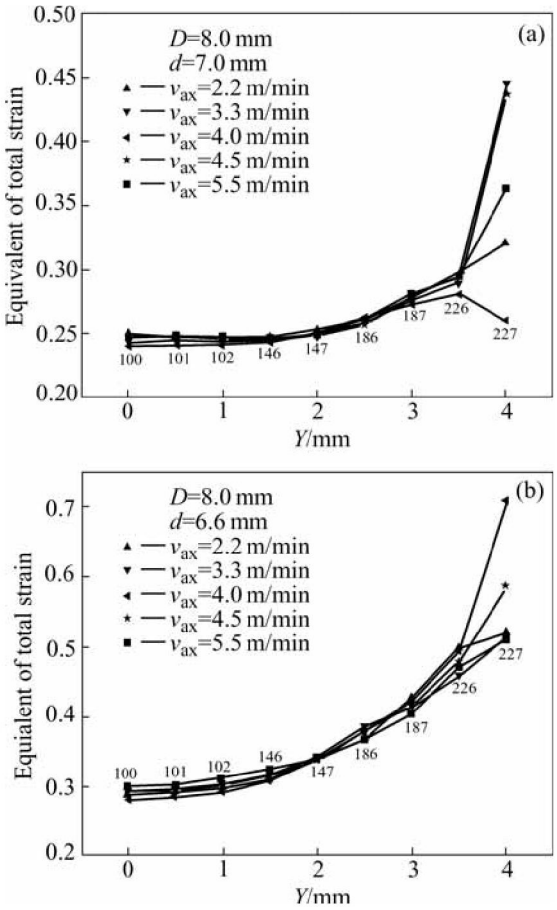

Fig.6 Path plot of equivalent strain along radial direction: (a) d=7.0 mm; (b) d= 6.6mm

conclusion can be drawn as that from Fig.6(a). Under various conical feeding angle, the magnitude of v_{ax} has no notable influence on the homogeneity of the strain distribution along the radial direction. So the change of v_{ax} has no obvious influence on the homogeneity of the strain distribution along the radial direction. This phenomenon arises from the fact that the magnitude of v_{ax} influences not the total strain of nodes but the strain in single loading impact (see Figs.3(b), (c) and (d)), and the total strain under various v_{ax} is of the same.

3.5 Surface roughness and guide line to selection of v_{ax}

The rating parameter R_z of the surface roughness describes the profile irregularity. According to the definition, the height of spiral spine-like ridge 'A' is equivalent to R_z and so it can be used to describe the surface roughness of the swaged bars.

Fig.7 shows the relation between 'A' and v_{ax} with different radial compression ratios. Fitted with quadratic polynomial, the correlation coefficients are relatively 0.993 and 0.989 8, which indicates that under various radial compression ratios the 'A' and the v_{ax} meet the parabolic relation (see Fig.7):

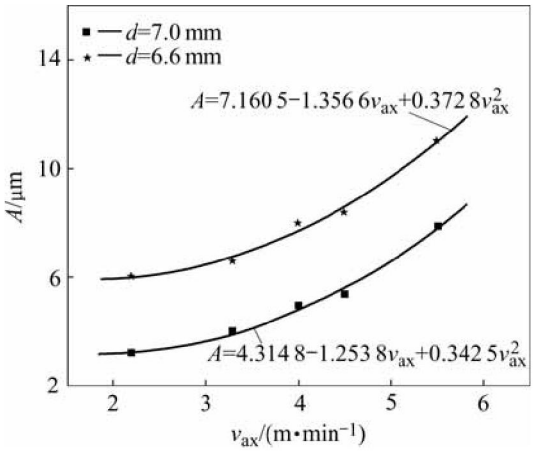

Fig.7 Correlation between height of spiral spine-like ridges and v_{ax}

$$A = av_{ax}^2 + bv_{ax} + c \tag{3}$$

In Eqn.(3), when the v_{ax} equals to its minimum v_{ax}= $-[b/(-2a)]$, the A reaches its minimum A_{min}= $c-b^2/4a$. So when the other processing parameters (except for v_{ax}) remains fixed, there exists a $v_{ax,\ min}$ below which the decrease of the v_{ax} will no longer improve the surface

roughness. When d=6.6 mm, $v_{ax,\ min}$=1.82 m/min, and when d=7.0 mm, $v_{ax,\ min}$=1.83 m/min. To improve the production efficiency, the axial feeding velocity should be maximized under the precondition that the required surface roughness is meted. Commonly, when the end products are fabricated, the surface roughness R_a=3.2 (i.e. A=R_z=12.5) is necessary and substituting this value to Eqn.(3) yidelds the maximum v_{ax}. When d=6.6 mm, $v_{ax,\ max}$=6.02 m/min, and when d=7.0 mm, $v_{ax,\ max}$=7.05 m/min.

4 Test of validity of rotary swaging model

Practical swaging processing is performed with a swaging machine (B202) and all the processing parameters are the same as the simulated. Diameters of the swaging products are measured with a tool microscope (19JA) and forty values are acquired for every swaging product. So the experimental radial displacements of nodes at the exterior surface are: Δy= −(8.0−d)/2.

Thus the height of the spiral spine-like ridges can be calculated through the path plot of the radial displacement along axial direction (see Fig.5(b)) by

$$A = \overline{A}_{\text{peak}} - \overline{A}_{\text{valley}} \tag{4}$$

where A is the height of the spiral spine-like ridges, $\overline{A}_{\text{peak}}$ the average of the peak of the pulse, and $\overline{A}_{\text{valley}}$ the average of the valley of the pulse. Table 2 shows the comparison of the simulated and measured height of the spiral spine-like ridges. The errors are below 8.0% which validates the FEA model of the swaging model developed.

Table 2 Comparison between simulated and measured height of spiral spine-like ridges (D=8.0 mm, d=7.0 mm)

Axial feeding velocity, v_{ax}/(m·min^{-1})	Simulated height/μm	Experimental height/μm	Error/%
3.3	4.00	4.3	7.0
4.5	5.37	5.8	7.4
5.5	7.85	8.5	7.6

5 Conclusions

1) The radial displacement that occurs in one pulse impact is in direct proportion to v_{ax}. At low v_{ax}, the total deformation of each node is achieved through many times of saddening.

2) The height of the spiral spine-like ridge 'A' is equivalent to the surface roughness rating parameter R_Z. When the other processing parameters (except for v_{ax}) remains fixed, A is in parabolic relation to the v_{ax} and there exists a minimum $v_{ax,\ min}$ below which the decrease of the v_{ax} will no longer improve the surface roughness. When d=6.6 mm, $v_{ax,\ min}$=1.82 m/min, and when d=7.0 mm, $v_{ax,\ max}$=1.83 m/min.

3) v_{ax} should be maximized to improve the production efficiency under the precondition that the required surface roughness is met. If R_a=3.2 (i.e. R_z= 12.5) is required for the end product, then $v_{ax,\ max}$=6.02 m/min is gotten for d=6.6 mm and $v_{ax,\ max}$=7.05 m/min for d=7.0 mm.

4) The magnitude of v_{ax} has no notable influence on the homogeneity of strain distribution along radial direction and so on the level of the following two defects viz. pits at the end of the product, and insufficient forging at the core of the swaging products.

References

[1] LIN Fa-yu. Special Forging Technology [M]. Beijing: Mechanical Industry Press, 1991. 150−170. (in Chinese)

[2] JIN Wen-zhong, LIU Shun-hua, LIU Li-ming. Research for structure, performance and shaping technical of magnesium alloys welding wire [J]. Metal Forming Technology, 2003, 21(6): 73−82. (in Chinese)

[3] YOSHIHARA S, MAC DONALD B, HASEGAWA T. Design improvement of spin forming of magnesium alloy tubes using finite element [J]. Journal of Materials Processing Technology, 2004, 153−154: 816−820.

[4] CHEN Fuh-kuo, HUANG Tyng-bin, CHANG Chih-kun. Deep drawing of square cups with magnesium alloy AZ31 sheets [J]. International Journal of Machine Tools & Manufacture, 2003, 43: 1553−1559.

[5] HARIHARASUDHAN P, GRACIOUS N, TAYLAN A. Finite element simulation of magnesium alloy sheet forming at elevated temperatures [J]. Journal of Materials Processing Technology, 2004, 146: 52−60.

[6] YOSHIHARA S, MACDONALD B J, NISHIMURA H. Optimisation of magnesium alloy stamping with local heating and cooling using the finite element method [J]. Journal of Materials Processing Technology, 2004, 153/154: 319−322.

[7] CHUNG S W, KIM W J, HIGASHI K. The effect of die geometry on the double shear extrusion by parametric FVM simulation [J]. Scripta Materialia, 2004, 51: 1117−1122.

[8] WANG Ling-yun, SONG Mei-juan, LIU Rao-chuan. Superplasticity and superplastic instability of AZ31B magnesium alloy sheet [J]. Transa Nonferrous Met Soc China, 2006, 16: 327−332.

[9] MICHAEL M AVEDESIAN. ASM Specialty Handbook-Magnesium and Magnesium Alloys [M]. USA: ASM, 1999. 1−11.

[10] RONG Li, NIE Zuo-ren, DU Wen-bo, ZUO Tie-yong. Symposium of Forum for China Magnesium Industry Development [M]. Beijing: China Magnesium Association, 2004. 122−128. (in Chinese)

[11] MSC Software Corporation. MSC. Marc 2001(Volume C): Program Input [M]. USA: MSC Software Corporation, 2001. 1668−1759.

[12] ZNCROPERA F P. Fundamentals of Heat Transfer [M]. GE Xin-shi, transl. Hefei: Anhui Educational Press, 1985.

[13] YU Han-qing. Surface Roughness and Its Measurement [M]. Beijing: Standard Press of China, 1987. 47−86. (in Chinese)

(Edited by LONG Huai-zhong)